applied sciences

MDPI

Article

Phonons and Thermal Transport in Si/SiO_2 Multishell Nanotubes: Atomistic Study

Calina Isacova [1], Alexandr Cocemasov [1], Denis L. Nika [1,*] and Vladimir M. Fomin [1,2,3]

[1] E. Pokatilov Laboratory of Physics and Engineering of Nanomaterials, Department of Physics and Engineering, Moldova State University, MD-2009 Chisinau, Moldova; isacova.calina@gmail.com (C.I.); kocemasov@live.ru (A.C.); v.fomin@ifw-dresden.de (V.M.F.)
[2] Institute for Integrative Nanosciences, Leibniz Institute for Solid State and Material Research Dresden, D-01069 Dresden, Germany
[3] Moscow Engineering Physics Institute, National Research Nuclear University, Moscow 115409, Russia
* Correspondence: dlnika@yahoo.com; Tel.: +373-67560423

Featured Application: Multishell nanotubes are promising candidates for an advancement in thermoelectric materials and devices.

Abstract: Thermal transport in the Si/SiO_2 multishell nanotubes is investigated theoretically. The phonon energy spectra are obtained using the atomistic lattice dynamics approach. Thermal conductivity is calculated using the Boltzmann transport equation within the relaxation time approximation. Redistribution of the vibrational spectra in multishell nanotubes leads to a decrease of the phonon group velocity and the thermal conductivity as compared to homogeneous Si nanowires. Phonon scattering on the Si/SiO_2 interfaces is another key factor of strong reduction of the thermal conductivity in these structures (down to 0.2 $Wm^{-1}K^{-1}$ at room temperature). We demonstrate that phonon thermal transport in Si/SiO_2 nanotubes can be efficiently suppressed by a proper choice of nanotube geometrical parameters: lateral cross section, thickness and number of shells. We argue that such nanotubes have prospective applications in modern electronics, in cases when low heat conduction is required.

Keywords: multishell nanotubes; phonons; thermal transport; lattice-dynamics approach

Citation: Isacova, C.; Cocemasov, A.; Nika, D.L.; Fomin, V.M. Phonons and Thermal Transport in Si/SiO_2 Multishell Nanotubes: Atomistic Study. *Appl. Sci.* **2021**, *11*, 3419. https://doi.org/10.3390/app11083419

Academic Editor: Andrea Li Bassi

Received: 26 March 2021
Accepted: 8 April 2021
Published: 11 April 2021

1. Introduction

Rapid miniaturization of electronic devices and increasing power consumption require an efficient heat management at nanoscale [1,2]. Thermal properties of nanostructures and different methods of their optimization have been widely investigated both experimentally and theoretically [3–8]. Phonon engineering, i.e., targeted modification of phonon modes in nanostructures to enhance their thermal [5,9,10], electrical [9] and optical properties [11,12], manifests itself as a powerful tool for the optimization of nanoscale thermal transport [5,9,10]. Nanomaterials with high thermal conductivity (TC), such as graphene, are promising candidates as heat spreaders and interconnectors [13–16], while nanomaterials with low thermal conductivity and high electrical conductivity can be used for thermoelectric applications. The efficiency of the thermoelectric energy conversion, figure of merit ZT, is directly proportional to the electrical conductivity and inversely proportional to the total thermal conductivity: $ZT = S^2\sigma T/\left(\kappa_{ph} + \kappa_{el}\right)$, where S is the Seebeck coefficient, σ is the electrical conductivity, T is the absolute temperature, and κ_{ph} and κ_{el} are the phonon and electron thermal conductivities, respectively. Acoustic phonons are the main heat carriers in bulk semiconductors at room temperature (RT) and above. Strong spatial confinement of acoustic phonons in nanostructures significantly changes phonon energy spectra as compared with the bulk case, resulting in a decrease of phonon group velocities [17–23]. The latter, in combination with an enhancement of phonon boundary

scattering, stipulates a reduction of the lattice TC in nanostructures in comparison with that in bulk materials [9,17,18,20,22]. A significant reduction of the thermal conductivity leads to an increase of ZT, e.g., in Bi_2Te_3 quantum-well structures ZT increases up to 13 times in comparison with the bulk value [24]. The silicon-based nanostructures are also prospective for thermoelectric applications despite the fact that bulk silicon is a poor thermoelectric with $ZT \sim 0.01$ at RT [25]. Hochbaum et al. [26] and Boukai et al. [27] demonstrated that significant increase of ZT occurs in Si nanowires (NWs) due to suppression of phonon transport. Strong reduction of lattice thermal conductivity in cross-sectional modulated Si nanowires [28–30] may also lead to improvement of their thermoelectric efficiency as compared with bulk Si. A reduction of RT TC down to 1 $Wm^{-1}K^{-1}$ was also reported for SiGe nanocomposite materials [3,31]. It was shown [3] that a rise of the Seebeck coefficient is stronger than a possible increase of the electrical resistivity.

Si-based nanotubes (NTs) are even more promising for thermoelectric applications due to a very large surface-to-volume ratio. It was shown in a molecular dynamics study [32] that RT thermal conductivity of Si NTs is as small as about 33 percent of that of Si NW with the same cross section area. In p-type Si NTs, a five-fold enhancement of ZT ($ZT = 0.34$ at 550 °C) was experimentally achieved as compared to the bulk counterpart [33]. Considerable advancements were also achieved in the methods of large-scale and low-cost preparation of Si NTs. A template-free preparation by an electrochemical method with in-situ surface modification of Si NTs was reported in Ref. [34]. In Ref. [35], a low-cost fabrication technology of vertically aligned Si NTs via a wet-etching process with controllable NT thickness was demonstrated. Besides thermoelectrics, the applications of Si-based NTs include biosensors, energy storage, photodetectors, optoelectronics and field-effect transistors [35–39].

Efficient engineering of the acoustic phonon energy spectrum is carried out in self-rolled micro- and nanoarchitectures [40]. The strain-driven roll-up procedure is a powerful high-tech instrument for fabrication of multilayer micro- and nano-superlattices and their arrays [41–43]. The acoustic phonon dispersion in multishell tubular nanostructures has been analyzed within the framework of elastodynamics [44]. It was shown that the number of shells is an important control parameter of the phonon dispersion together with the structure dimensions and acoustic impedance mismatch between the shells. An increase of the number of shells was shown to lead to an appreciable decrease of the average and root-mean-square phonon group velocities. A strong reduction of lattice thermal conductivity in low-dimensional nanostructures (nanowires, thin films and superlattices) compared with corresponding bulk materials justified diverse proposals to use them for thermoelectric and thermal insulating applications [17,22,26–30].

Silica is a commonly used matrix material at preparation of different nanostructures and nanomaterials [45–50]. Moreover, combination of crystalline silicon and amorphous silica layers allows one to study unusual phonon phenomena related to phonon propagation through heterogeneous crystalline/amorphous media [8,28,43,51]. Although Si-based NTs have been intensively studied during recent years [32–39], their thermal properties remain poorly understood.

In the present paper, we develop an atomistic calculation to tackle the phonons and thermal transport in novel Si/SiO_2 multishell nanotubes (MNTs). We demonstrate that phonon thermal transport in Si/SiO_2 MNTs can be efficiently suppressed by a proper choice of a nanotube's geometrical parameters: lateral cross section, thickness and number of shells. Our results also shed light on the interplay between different mechanisms of phonon scattering.

The remainder of the paper is organized as follows. In Section 2, we describe our theoretical model employed for calculations of phonon energy dispersion and the lattice thermal conductivity in Si/SiO_2 MNTs. Discussions of the obtained results on phonon modes and thermal transport in Si/SiO_2 MNTs are provided in Section 3. Conclusions are given in Section 4.

2. Theoretical Model of Thermal Conductivity in Si/SiO_2 Multishell Nanotubes

We study rectangular MNTs formed from alternating layers of silicon and silica. The number of Si/SiO_2 bilayer shells is varied. A scheme of a MNT is shown in Figure 1. The external surface of the nanotube is assumed to be free [8,19,21]. The X and Y axes of the Cartesian coordinate system are located in the cross-sectional plane of the NT and are parallel to its sides, while the Z axis is directed along the NT axis. We assume that the NT is infinite along the Z axis. The thicknesses of the shells are denoted $d_{x,Si}$ and $d_{y,Si}$ for silicon (d_{x,SiO_2} and d_{y,SiO_2} for silicon dioxide), while the cavity dimensions are $d_{x,cavity}$ and $d_{y,cavity}$. The number of Si/SiO_2 bilayer shells is denoted by N.

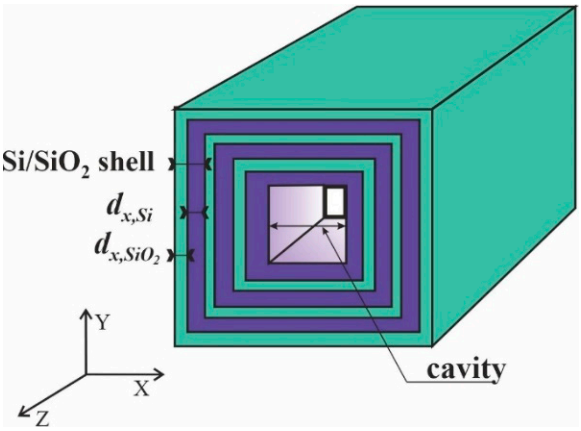

Figure 1. Scheme of a Si/SiO_2 rectangular MNT.

The phonon energy spectra in the Si/SiO_2 MNTs and Si NWs are calculated using an atomistic face-centered cubic cell (FCC) model within the lattice dynamics approach [8]. In the FCC model, the diamond-type crystal lattice, consisting of two shifted face-centered cubic Bravais sublattices, is replaced with one face-centered cubic lattice with all atoms possessing a doubled mass. The equations of motion for atoms in the harmonic approximation is [28]:

$$m_i\omega^2 u_\alpha\left(\vec{r}_i, \vec{q}\right) = \sum_{\beta=x,y,z;\ \vec{r}_j} D_{\alpha\beta}\left(\vec{r}_i, \vec{r}_j\right) u_\beta\left(\vec{r}_j, \vec{q}\right), \alpha = x, y, z \quad (1)$$

Here, i enumerates atoms in a NT translation period (two cross-sectional atomic planes in case of FCC model), m_i is the mass of the i-th atom, $\vec{r}_i$ and $\vec{r}_j$ are the radius vectors of the i-th and j-th atoms, respectively, $\vec{q}$ is the phonon wavevector, ω is the sought phonon frequency, $u_\alpha\left(\vec{r}_i, \vec{q}\right)$ is a component of the displacement vector for the i-th atom and the dynamic matrix $D_{\alpha\beta}\left(\vec{r}_i, \vec{r}_j\right)$ is

$$D_{\alpha\beta}\left(\vec{r}_i, \vec{r}_j\right) = \Phi_{\alpha\beta}\left(\vec{r}_i, \vec{r}_j\right) / \sqrt{m_i m_j} \quad (2)$$

where m_j is the mass of the j-th atom and $\Phi_{\alpha\beta}\left(\vec{r}_i, \vec{r}_j\right)$ is the matrix of force constants. In the FCC model, the summation in Equation (1) is performed over all the nearest and second-nearest atoms of the i-th atom: twelve nearest atoms at $\vec{r}_j = \vec{r}_i + \vec{h}_j^{\,I}$ (j = 1, . . . , 12) and six second-nearest atoms at $\vec{r}_j = \vec{r}_i + \vec{h}_j^{\,II}$ (j = 1, . . . , 6) [8,28]. The components of the vectors $\vec{h}_j^{\,I}$ and $\vec{h}_j^{\,II}$ are presented in Table I of Ref. [28]. The force constant matrix $\Phi_{\alpha\beta}\left(\vec{r}_i, \vec{r}_j\right)$ used in our calculations is taken from Ref. [8]:

$$\Phi^{(1)}_{\alpha\beta}\left(\vec{h}^{(k)}, \vec{r}_k, \vec{r}'_k\right) = \frac{-\kappa_1\left(\vec{r}_k, \vec{r}'_k\right) h^{(k)}_\alpha h^{(k)}_\beta}{\left|\vec{h}^{(k)}\right|^2} \tag{3}$$

$$\Phi^{(2)}_{\alpha\beta}\left(\vec{h}^{(k)}, \vec{r}_k, \vec{r}'_k\right) = \begin{pmatrix} \kappa_2\left(\vec{r}_k, \vec{r}'_k\right) & 0 & 0 \\ 0 & \kappa_3\left(\vec{r}_k, \vec{r}'_k\right) & 0 \\ 0 & 0 & \kappa_3\left(\vec{r}_k, \vec{r}'_k\right) \end{pmatrix} \text{ for atoms with coordinates } (\pm a, 0, 0)$$

$$\Phi^{(2)}_{\alpha\beta}\left(\vec{h}^{(k)}, \vec{r}_k, \vec{r}'_k\right) = \begin{pmatrix} \kappa_3\left(\vec{r}_k, \vec{r}'_k\right) & 0 & 0 \\ 0 & \kappa_2\left(\vec{r}_k, \vec{r}'_k\right) & 0 \\ 0 & 0 & \kappa_3\left(\vec{r}_k, \vec{r}'_k\right) \end{pmatrix} \text{ for atoms with coordinates } (0, \pm a, 0) \tag{4}$$

$$\Phi^{(2)}_{\alpha\beta}\left(\vec{h}^{(k)}, \vec{r}_k, \vec{r}'_k\right) = \begin{pmatrix} \kappa_3\left(\vec{r}_k, \vec{r}'_k\right) & 0 & 0 \\ 0 & \kappa_3\left(\vec{r}_k, \vec{r}'_k\right) & 0 \\ 0 & 0 & \kappa_2\left(\vec{r}_k, \vec{r}'_k\right) \end{pmatrix} \text{ for atoms with coordinates } (0, 0, \pm a)$$

This matrix depends on 3 independent force constants κ_1, κ_2 and κ_3, which can be expressed through the elastic moduli c_{11}, c_{12} and c_{44} of a bulk cubic crystal [8]: $\kappa_1 = \frac{a(c_{12}+c_{44})}{2}$, $\kappa_2 = \frac{a(c_{11}-c_{12}-c_{44})}{4}$, $\kappa_3 = \frac{a(c_{44}-c_{12})}{8}$, where a is the lattice constant.

Calculation of the thermal conductivity of Si/SiO_2 MNTs and Si NWs is conducted using the following formula:

$$\kappa_{ph} = \frac{1}{2\pi k_B T^2 S_{NT}} \sum_s \int_0^{q_{z,max}} [\hbar\omega_s(q_z) v_{z,s}(q_z)]^2 \tau_{tot,s}(q_z) \frac{\exp\left(\frac{\hbar\omega_s(q_z)}{k_B T}\right)}{\left[\exp\left(\frac{\hbar\omega_s(q_z)}{k_B T}\right) - 1\right]^2} dq_z \tag{5}$$

This expression was derived from the Boltzmann transport equation within the relaxation-time approximation [6,22,52,53] and captured the quasi one-dimensional density of the phonon states. In Equation (5), the summation is performed over all phonon branches $s = 1, \ldots, N_b$, S_{NT} is the NT cross-sectional area, ω_s is the phonon frequency, $v_{z,s}$ is the Z-th component of the phonon group velocity, $q_{z,max} = \pi/a$ is the maximal amplitude of phonon wavevector, $\tau_{tot,s}$ is the total phonon relaxation time, k_B is the Boltzmann constant, $\hbar$ is the Planck constant and T is the temperature.

The total phonon relaxation rate was estimated according to the Matthiessen's rule:

$$\tau^{-1}_{tot,s}(q_z) = \tau^{-1}_{U,s}(q_z) + \tau^{-1}_{imp,s}(q_z) + \tau^{-1}_{x,s}(q_z). \tag{6}$$

Here, $\tau_{U,s}$ is the relaxation time for the Umklapp scattering: $\tau^{-1}_{U,s}(q_z) = B[\omega_s(q_z)]^2 T \exp(-C/T)$ [22] and $\tau_{imp,s}$ is the relaxation time for the phonon-impurity scattering: $\tau^{-1}_{imp,s}(q_z) = A[\omega_s(q_z)]^4$, where $A = 1.32 \times 10^{-45}$ s^3 is determined analytically from the isotope concentration of natural silicon [8,22]. Parameters $B = 1.73 \times 10^{-19}$ sK^{-1} and $C = 137.3$ K of the Umklapp scattering are fitted to reproduce experimental temperature dependence of bulk Si thermal conductivity [54]. In Si/SiO_2 MNTs, both phonon-boundary scattering at Si/SiO_2 interfaces and diffusion of vibrational excitations in amorphous SiO_2 influence the thermal conductivity. To analyze the role of these mechanisms in thermal transport, we performed calculations of the thermal conductivity using different values of

the third term in Equation (6). We employed the "effective scattering rate" $\tau_{SiO_2}^{-1}$ due to the diffusion of vibrational excitations in amorphous SiO_2 [43]:

$$\frac{1}{\tau_{x,s}} = \frac{1}{\tau_{SiO_2,s}(q_z)} = v_{z,s}^2(q)\frac{3\omega_s(q)}{a_{b.l.}^2 F\langle\omega\rangle^2}\frac{d_{x,SiO_2}}{d_{x,Si}} \quad (7)$$

or the relaxation rate for the boundary scattering τ_B^{-1}:

$$\frac{1}{\tau_{x,s}} = \frac{1}{\tau_{B,s}(q_z)} = \frac{1-p}{1+p}\frac{|v_{z,s}(q_z)|}{2}N\left(\frac{1}{d_{x,Si}} + \frac{1}{d_{y,Si}} + \frac{1}{d_{x,SiO_2}} + \frac{1}{d_{y,SiO_2}}\right) \quad (8)$$

or took into account both of them: $1/\tau_{x,s} = 1/\tau_{SiO_2,s} + 1/\tau_{B,s}$. In Equations (7) and (8) $a_{b.l.} = 0.235$ nm is the SiO_2 bond length, $\langle\omega\rangle$ is the mean vibrational frequency (the mean vibrational energy $\hbar\langle\omega\rangle = 34$ meV is taken from Ref. [43]), $F = 0.33$ according to Ref. [55]. The specularity parameter p characterizes the phonon-boundary scattering. Depending on the boundary roughness, p can take values between $p = 0$ (pure diffusive scattering) and $p = 1$ (pure specular scattering).

3. Results and Discussion

We calculated the phonon energy spectra in Si/SiO_2 MNTs and Si NWs by solving Equation (1) numerically (eigenvalue problem). Diagonalization of the matrix from Equation (1) was performed using LAPACK library [56] under GCC 8.4 compiler [57]. The calculations were performed for all q_z in the interval $(0, \frac{\pi}{a})$.

In 1D case, the partial phonon density of states (DOS) per unit length in real space can be found from the relation: $g_s(\omega)d\omega = \frac{1}{2\pi}dq_{z,s}$. Hence, the (total) phonon DOS per unit length in real space is given by:

$$g(\omega) = \sum_{s(\omega)} g_s(\omega) = \sum_{s(\omega)} \frac{1}{2\pi v_{z,s}}, \quad (9)$$

where summation is performed over all phonon modes $s(\omega)$ with frequency ω. The phonon energy spectra and total DOS for Si NW and Si/SiO_2 MNTs are shown in Figure 2. The Si NW has dimensions 11 ML × 11 ML (2.97 nm × 2.97 nm; 1 monolayer (ML) = 0.27 nm). The geometric parameters of the Si/SiO_2 NTs are as follows: the cavity cross section is 45 ML × 45 ML (12.15 nm × 12.15 nm), the thickness of the Si layer is 6 ML (1.62 nm) and the thickness of the SiO_2 layer is 4 ML (1.08 nm). Panel (a) represents results for the Si NW, panel (b)–for the NT with a single Si/SiO_2 bilayer shell ($N = 1$) and panel (c)–for the NT with two Si/SiO_2 bilayer shells ($N = 2$). Similarly to rectangular nanowires [21,58], phonon modes in rectangular MNTs can be classified into four types according to the spatial symmetry of the displacement vector components: Dilatational, $Flexural_1$, $Flexural_2$ and Shear. For the Si NW, we show phonon branches with numbers s = 1–4, 11, 17, . . . , 47, 51, 76, . . . , 301, 320 for Shear polarization; s = 1–4, 11, 17, . . . , 47, 51, 76, . . . , 326, 342 for Dilatational polarization and s = 1–4, 11, 17, . . . , 47, 51, 76, . . . , 326, 331 for $Flexural_1$ and $Flexural_2$ polarizations. For the Si/SiO_2 NT with $N = 1$, we present phonon branches with s = 1–5, 30, 55, 480, 500, 550, . . . , 1000, 1075, . . . , 1600, 1661 for Dilatational polarization; s = 1–5, 30, 55, 480, 500, 550, . . . , 1000, 1075, . . . , 1600, 1640 for Shear polarization and s = 1–5, 30, 55, 480, 500, 550, . . . , 1000, 1075, . . . , 1600, 1650 for $Flexural_1$ and $Flexural_2$ polarizations. For the Si/SiO_2 NT with $N = 2$, the following phonon branches are depicted: s = 1–5, 80, 155, 230, 305, 380, 455, 500, 675, 850, . . . , 2950, 3000, 3100 . . . , 3900, 3920 for Dilatational polarization; s = 1–5, 80, 155, 230, 305, 380, 455, 500, 675, 850, . . . , 2950, 3000, 3100 . . . , 3800, 3880 for Shear polarization and s = 1–5, 80, 155, 230, 305, 380, 455, 500, 675, 850, . . . , 2950, 3000, 3100, . . . , 3900 for $Flexural_1$ and $Flexural_2$ polarizations.

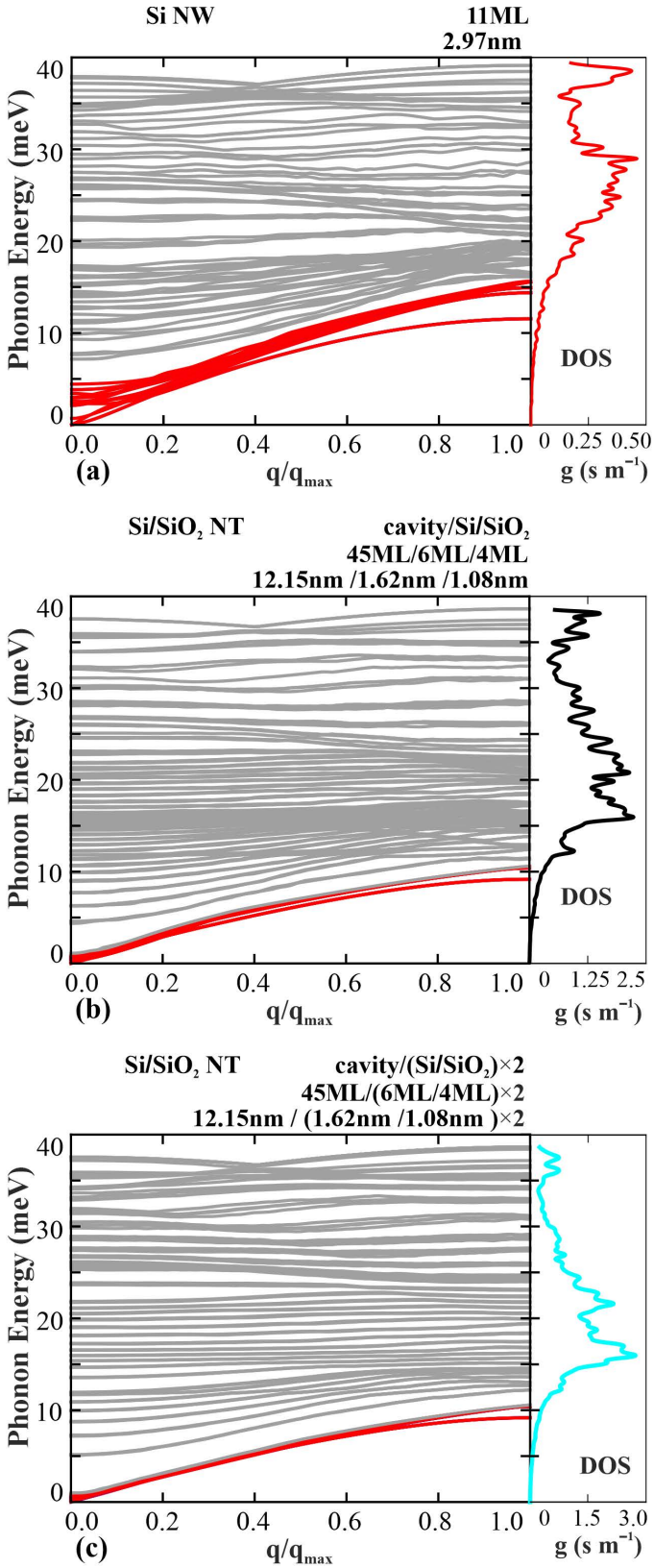

Figure 2. Phonon dispersions and phonon density of states in the Si NW with the cross section 11 ML × 11 ML (panel (**a**)); in the Si/SiO_2 NTs (nanotubes) with the cavity cross section 45 ML × 45 ML and a single Si/SiO_2 bilayer shell (panel (**b**)) and two Si/SiO_2 bilayer shells (panel (**c**)). The thicknesses of silicon and silica layers in the Si/SiO_2 bilayer are 6 ML and 4 ML, correspondingly.

The number of confined phonon branches in the NTs (N_b = 6600 for a single-shell NT and N_b = 15,600 for a double-shell NT) is substantially larger than that in a NW (N_b = 1323). The slope of the lowest phonon branches in NTs is smaller than that in a NW due to acoustic mismatch between silicon and silicon dioxide. A great number of phonon modes in the NTs with energy $\hbar\omega > 10$ meV are nearly dispersionless and possess group velocities close to zero. As compared to a NW, the DOS maximum in NTs is shifted toward the lower energy interval, where the drop of the average phonon group velocity is more significant (see Figure 3). The DOS maximum in a MNT with two bilayer shells is more prominent due to a larger number of phonon modes concentrated in SiO_2, which possess a smaller maximal phonon energy than Si.

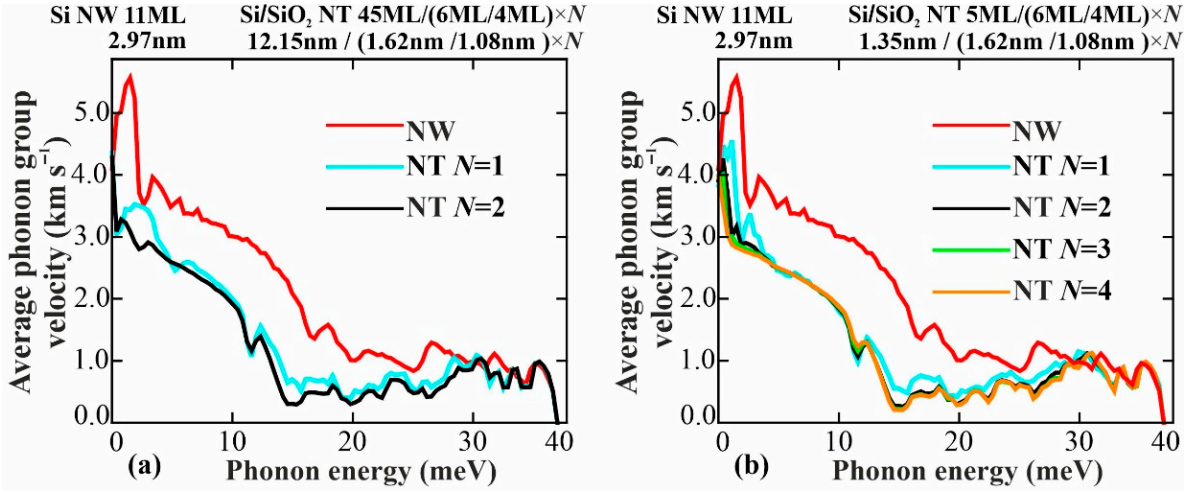

Figure 3. Average phonon group velocities as a function of phonon energies in Si/SiO_2 MNTs with the cavity cross section 45 ML × 45 ML (**a**) and 5 ML × 5 ML (**b**) and different numbers of Si/SiO_2 bilayer shells, formed by silicon layer with thickness 6 ML and silica layer with thickness 4 ML. Results for Si NW with cross section 11 ML × 11 ML are also shown for comparison.

The effect of phonon deceleration in MNTs with different numbers of Si/SiO_2 bilayer shells (N = 1, 2, 3, 4) is illustrated in Figure 3, where the average phonon group velocity $\langle v \rangle(\omega) = \sum_{s(\omega)}(v_{z,s}g_s(\omega))/\sum_{s(\omega)} g_s(\omega)$ is shown as a function of the phonon energy for a Si NW with cross section $N_x \times N_y$ = 11 ML × 11 ML and different Si/SiO_2 NTs with the following geometrical parameters: $N_{cavity,x} \times N_{cavity,y}$ = 45 ML × 45 ML, $N_{Si,x} = N_{Si,y}$ = 6 ML, $N_{SiO_2,x} = N_{SiO_2,y}$ = 4 ML (panel (a)) and $N_{cavity,x} \times N_{cavity,y}$ = 5 ML × 5 ML, $N_{Si,x} = N_{Si,y}$ = 6 ML, $N_{SiO_2,x} = N_{SiO_2,y}$ = 4 ML (panel (b)). The phonon group velocity in NTs is smaller than that in a NW over a wide energy range (0 to 30 meV). The reduction of the phonon group velocities in NTs is explained by an acoustic mismatch between Si and SiO_2, a stronger phonon confinement and a spectral redistribution of the phonon DOS in NTs. In the energy range from 30 to 37 meV, the phonon group velocities vary near the same low values for all considered NTs. Increase of the number of shells slightly reinforces the drop of phonon group velocity.

A comparison of temperature dependencies of thermal conductivity (TC) in a Si NW and Si/SiO_2 MNTs is provided in Figure 4. The geometrical parameters of a NW and MNTs are the same as in Figure 3. The thermal conductivity curves presented in panels (b) and (e) are calculated considering diffusion transport in SiO_2 (see Equation (7)), while those in panels (a) and (d) consider boundary scattering (see Equation (8)) with the specularity parameter p = 0.6. The values of the thermal conductivity in the NTs (even for the NTs with a greater number of phonon modes) are lower than the thermal conductivity in the NW in the whole temperature range. This decrease of TC in the MNTs is due to modification of phonon energy spectra in MNTs leading to phonon deceleration, as well as enhancement of the phonon scattering at interfaces and diffusion of vibrational excitations in SiO_2 layers.

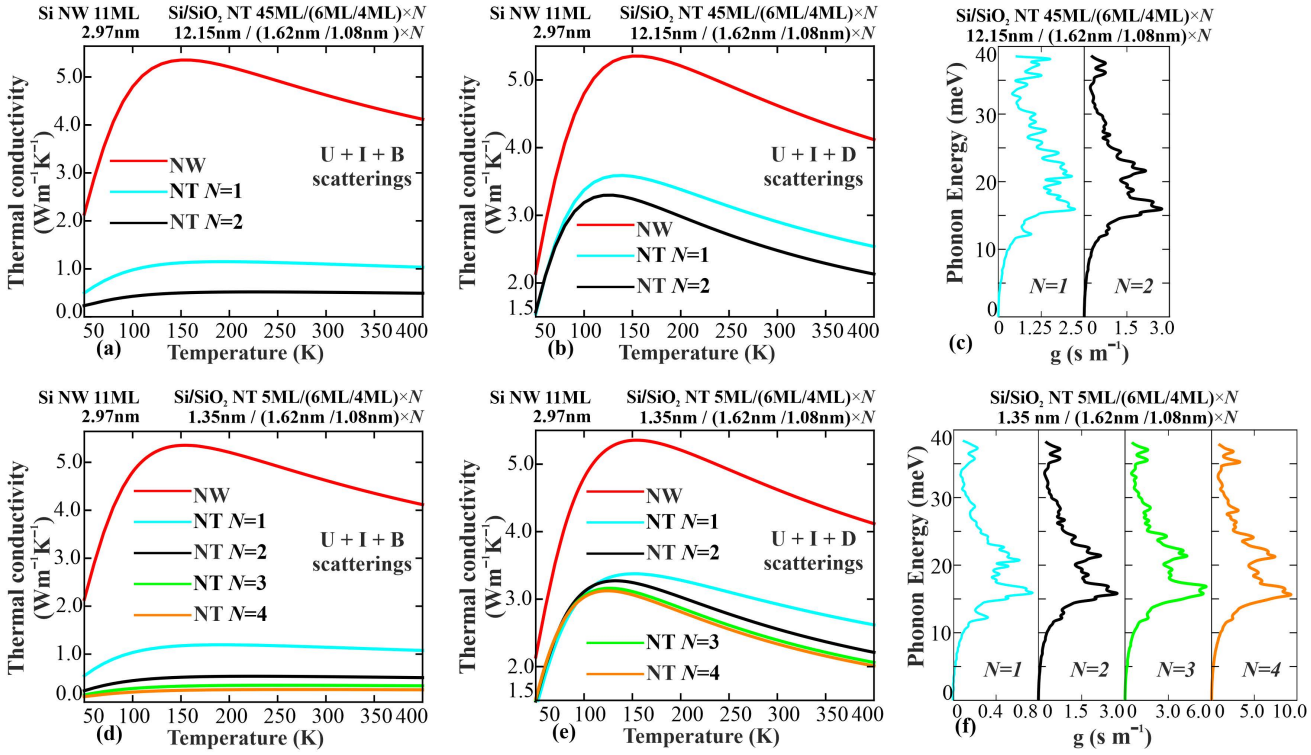

Figure 4. Temperature dependence of the TC (thermal conductivity) (**a**,**b**,**d**,**e**) and phonon DOS (density of states) (**c**,**f**) in Si/SiO_2 MNTs. The TC is calculated considering the phonon Umklapp and boundary scatterings (**a**,**d**) as well as the phonon Umklapp scattering and "effective scattering rate" due to diffusion of vibrational excitations in SiO_2 (**b**,**e**).

The maxima of the thermal conductivity curves are determined by the interplay between three-phonon Umklapp and boundary or effective diffusion scatterings. At low temperatures, the phonon-boundary scattering or the diffusion of vibrational excitations in SiO_2 layers is the main mechanism of scattering, and the increase of TC with temperature is explained by the population of high-energy phonon modes. A subsequent rise of temperature results in the reinforcement of the Umklapp scattering and a reduction of TC. Additional interfaces between the shells effectively scatter phonons, hence the TC decreases with augmentation of the number of shells (see panels (a) and (d)) reaching values as low as 0.2 W/mK at RT for Si/SiO_2 NT with smaller cavity and $N = 4$. A similar dependence of TC on N was demonstrated experimentally for Si/SiO_2 rolled-up nanotubes of 1.9 μm to 3.2 μm radii and a 24-nm-thick shell [43]. The latter fact confirms the importance of our theoretical findings for an accurate prediction of thermal transport phenomena in Si/SiO_2 nanotubes in a wide range of lateral cross sections, numbers and thicknesses of the shells. However, the phonon dispersion and transport properties in multishell nanostructures with sizes of the order of a few hundred nm require further analysis because they are in the transitional region between the areas of applicability of elastodynamics and the atomistic approaches.

Usually, TC in nanostructures strongly depends on surface roughness and/or roughness of interfaces between layers in the case of multilayered nanostructures. Depending on the model, different values of the specularity parameter p were employed for the theoretical predictions and the interpretation of experimental results [28,29,52,59–62].

To elucidate the dependence of TC in MNTs on p, we plot in Figure 5a, the TC of a single-shell Si/SiO_2 NT (5 ML/6 ML/4 ML) as a function of temperature for different values of p. A decrease of the specularity parameter suppresses TC over the entire considered range of temperatures. Thus, the boundary scattering plays an important role in limiting thermal transport even for $T > 150$ K, where the three-phonon Umklapp scattering becomes relatively strong. This results in decreasing TC with T for $T > 150$ K. In Figure 5b, we show how different values of p affect the drop of TC in MNTs as compared with NWs.

The TC curves in Figure 5b were calculated taking into account both the phonon-boundary scattering and the diffusion of vibrational excitations in SiO_2 layers. Coexistence of the phonon-boundary scattering and the "effective scattering" due to the diffusion of vibrational excitations in SiO_2 layers results in lower values of TC in comparison with the cases of their separate action. At the same time, the TC reduction with rising number of shells remains manifested for different values of p (see Figure 5b). It is also worth noticing that for $p = 0.9$ the ratios between thermal conductivities in MNTs with different numbers of shells $\kappa_{ph}(N)/\kappa_{ph}(1)$ for $N = 2$ and 5 (see Figure 5c) are close to experimental values [43] despite the fact that experimental multishell NTs possess much larger sizes.

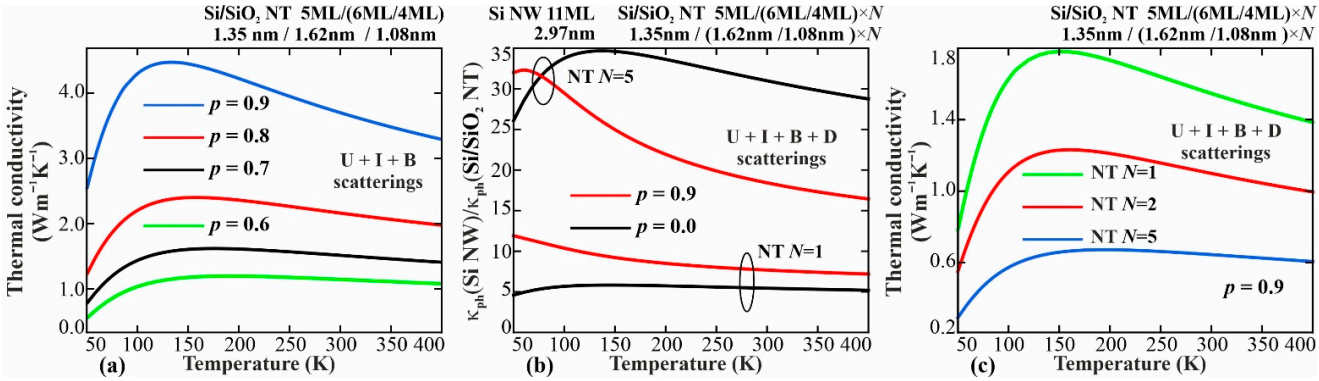

Figure 5. (**a**) TC in a single-shell Si/SiO_2 NT with dimensions 5 ML/(6 ML/4 ML) shown as a function of temperature for different values of p. (**b**) Ratio between thermal conductivities in Si NW and Si/SiO_2 MNTs reveals a significant drop of TC in MNTs. (**c**) TC in Si/SiO_2 MNTs with dimensions 5 ML/(6 ML/4 ML) $\times$ N at $N = 1, 2, 5$ shown as a function of temperature for $p = 0.9$.

4. Conclusions

Phonon and thermal properties of novel Si/SiO_2 multishell nanotubes are theoretically investigated within the lattice dynamics approach. It is demonstrated that the thermal conductivity in the Si/SiO_2 MNTs is by a factor of 5 to 35 lower than that in the corresponding Si NW as a function of the temperature, number of shells and the interface roughness. This effect is explained by the redistribution of phonon energy spectra in NTs leading to a stronger phonon confinement and a reduction of the average phonon group velocities. It is also established that a significant number of phonon modes are scattered on Si/SiO_2 interfaces, which enhances the influence of the phonon boundary scattering on the TC in the MNTs under analysis. As a result, the TC decreases with increase of the number of Si/SiO_2 shells. Low values of the TC in Si/SiO_2 MNTs as compared with other low-dimensional nanostructures make advanced semiconductor MNTs prospective candidates for thermoelectric applications.

Author Contributions: Conceptualization, D.L.N. and V.M.F.; software, C.I., A.C. and D.L.N.; validation, C.I., A.C., D.L.N. and V.M.F.; visualization, C.I.; writing—original draft preparation, C.I. and A.C.; writing—review and editing, D.L.N. and V.M.F.; funding acquisition and project administration, D.L.N. and V.M.F. All authors have read and agreed to the published version of the manuscript.

Funding: This research was funded by the German Research Foundation (DFG) grant # FO-956/4-1 and Moldova Agency for Research and Development grant #20.80009.5007.02.

Institutional Review Board Statement: Not applicable.

Informed Consent Statement: Not applicable.

Data Availability Statement: All the data are reported in the paper directly.

Acknowledgments: V.F. acknowledges a partial support through the MEPhI Academic Excellence Project (Contract # 02.a03.21.0005). C.I. is thankful for kind hospitality during her research stay at the IIN, IFW Dresden. The authors are grateful to O. G. Schmidt and G. Li for fruitful discussions.

Conflicts of Interest: The authors declare no conflict of interest. The funders had no role in the design of the study; in the collection, analyses, or interpretation of data; in the writing of the manuscript, or in the decision to publish the results.

References

1. Balandin, A.A. Nanoscale Thermal Management. *IEEE Potentials* **2002**, *21*, 11–15. [CrossRef]
2. Bar-Cohen, A.; Wang, P. On-chip thermal management and hot-spot remediation. In *Nano-Bio-Electronic, Photonic and MEMS Packaging*; Springer: Boston, MA, USA, 2010; pp. 349–429.
3. Dresselhaus, M.S.; Chen, G.; Tang, M.Y.; Yang, R.G.; Lee, H.; Wang, D.Z.; Ren, Z.F.; Fleurial, J.-P.; Gogna, P. New Directions for Low-Dimensional Thermoelectric Materials. *Adv. Mater.* **2007**, *19*, 1043–1053. [CrossRef]
4. Cahill, D.G.; Ford, W.K.; Goodson, K.E.; Mahan, G.D.; Majumdar, A.; Maris, H.J.; Merlin, R.; Phillpot, S.R. Nanoscale Thermal Transport. *J. Appl. Phys.* **2003**, *93*, 793–818. [CrossRef]
5. Balandin, A.A.; Nika, D.L. Phononics in Low-Dimensional Materials. *Mater. Today* **2012**, *15*, 266–275. [CrossRef]
6. Nika, D.L.; Pokatilov, E.P.; Askerov, A.S.; Balandin, A.A. Phonon Thermal Conduction in Graphene: Role of Umklapp and Edge Roughness Scattering. *Phys. Rev. B* **2009**, *79*, 155413. [CrossRef]
7. Kundu, A.; Mingo, N.; Broido, D.A.; Stewart, D.A. Role of Light and Heavy Embedded Nanoparticles on the Thermal Conductivity of SiGe Alloys. *Phys. Rev. B* **2011**, *84*, 125426. [CrossRef]
8. Nika, D.L.; Pokatilov, E.P.; Balandin, A.A.; Fomin, V.M.; Rastelli, A.; Schmidt, O.G. Reduction of Lattice Thermal Conductivity in One-Dimensional Quantum-Dot Superlattices Due to Phonon Filtering. *Phys. Rev. B* **2011**, *84*, 165415. [CrossRef]
9. Balandin, A.A. Nanophononics: Phonon Engineering in Nanostructures and Nanodevices. *J. Nanosci. Nanotechnol.* **2005**, *5*, 1015–1022. [CrossRef]
10. Cocemasov, A.I.; Isacova, C.I.; Nika, D.L. Thermal Transport in Semiconductor Nanostructures, Graphene, and Related Two-Dimensional Materials. *Chin. Phys. B* **2018**, *27*, 56301. [CrossRef]
11. Safavi-Naeini, A.H.; Van Thourhout, D.; Baets, R.; Van Laer, R. Controlling Phonons and Photons at the Wavelength Scale: Integrated Photonics Meets Integrated Phononics. *Optica* **2019**, *6*, 213–232. [CrossRef]
12. Nika, D.L.; Pokatilov, E.P.; Fomin, V.M.; Devreese, J.T.; Tempere, J. Resonant Terahertz Light Absorption by Virtue of Tunable Hybrid Interface Phonon–Plasmon Modes in Semiconductor Nanoshells. *Appl. Sci.* **2019**, *9*, 1442. [CrossRef]
13. Ghosh, S.; Bao, W.; Nika, D.L.; Subrina, S.; Pokatilov, E.P.; Lau, C.N.; Balandin, A.A. Dimensional Crossover of Thermal Transport in Few-Layer Graphene. *Nat. Mater.* **2010**, *9*, 555–558. [CrossRef] [PubMed]
14. Shao, Q.; Liu, G.; Teweldebrhan, D.; Balandin, A.A. High-Temperature Quenching of Electrical Resistance in Graphene Interconnects. *Appl. Phys. Lett.* **2008**, *92*, 202108. [CrossRef]
15. Horng, R.-H.; Lin, R.-C.; Hu, H.-L.; Peng, K.-C.; Hsu, C.-P. Diamond-Added-Copper Heat Spreader for UV LED Applications. *Electrochem. Solid State Lett.* **2011**, *14*, H453. [CrossRef]
16. Ko, G.; Kim, J. Semiconductor Devices, Materials, and Processing-Thermal Modeling of Graphene Layer on the Peak Channel Temperature of AlGaN/GaN High Electron Mobility Transistors. *IEEE-ECS Electrochem. Solid State Lett.* **2009**, *12*, H29. [CrossRef]
17. Balandin, A.; Wang, K.L. Significant Decrease of the Lattice Thermal Conductivity Due to Phonon Confinement in a Free-Standing Semiconductor Quantum Well. *Phys. Rev. B* **1998**, *58*, 1544. [CrossRef]
18. Colvard, C.; Gant, T.A.; Klein, M.V.; Merlin, R.; Fischer, R.; Morkoc, H.; Gossard, A.C. Folded Acoustic and Quantized Optic Phonons in (GaAl) As Superlattices. *Phys. Rev. B* **1985**, *31*, 2080. [CrossRef]
19. Balandin, A.A.; Pokatilov, E.P.; Nika, D.L. Phonon Engineering in Hetero-and Nanostructures. *J. Nanoelectron. Optoelectron.* **2007**, *2*, 140–170. [CrossRef]
20. Venkatasubramanian, R. Lattice Thermal Conductivity Reduction and Phonon Localizationlike Behavior in Superlattice Structures. *Phys. Rev. B* **2000**, *61*, 3091. [CrossRef]
21. Pokatilov, E.P.; Nika, D.L.; Balandin, A.A. Acoustic-Phonon Propagation in Rectangular Semiconductor Nanowires with Elastically Dissimilar Barriers. *Phys. Rev. B* **2005**, *72*, 113311. [CrossRef]
22. Mingo, N. Calculation of Si Nanowire Thermal Conductivity Using Complete Phonon Dispersion Relations. *Phys. Rev. B* **2003**, *68*, 113308. [CrossRef]
23. Pokatilov, E.P.; Nika, D.L.; Balandin, A.A. Acoustic Phonon Engineering in Coated Cylindrical Nanowires. *Superlattices Microstruct.* **2005**, *38*, 168–183. [CrossRef]
24. Hicks, L.D.; Dresselhaus, M.S. Effect of Quantum-Well Structures on the Thermoelectric Figure of Merit. *Phys. Rev. B* **1993**, *47*, 12727. [CrossRef] [PubMed]
25. Weber, L.; Gmelin, E. Transport Properties of Silicon. *Appl. Phys. A* **1991**, *53*, 136–140. [CrossRef]
26. Hochbaum, A.I.; Chen, R.; Delgado, R.D.; Liang, W.; Garnett, E.C.; Najarian, M.; Majumdar, A.; Yang, P. Enhanced Thermoelectric Performance of Rough Silicon Nanowires. *Nature* **2008**, *451*, 163–167. [CrossRef] [PubMed]

27. Boukai, A.I.; Bunimovich, Y.; Tahir-Kheli, J.; Yu, J.-K.; Goddard, W.A.; Heath, J.R. Silicon nanowires as efficient thermoelectric materials. In *Materials for Sustainable Energy*; Dusastre, V., Ed.; Macmillan Publishers Ltd.: London, UK; World Scientific Publishing Co. Pte. Ltd.: Singapore, 2010; pp. 116–119. ISBN 978-981-4317-64-1.
28. Nika, D.L.; Cocemasov, A.I.; Isacova, C.I.; Balandin, A.A.; Fomin, V.M.; Schmidt, O.G. Suppression of Phonon Heat Conduction in Cross-Section-Modulated Nanowires. *Phys. Rev. B* **2012**, *85*, 205439. [CrossRef]
29. Nika, D.L.; Cocemasov, A.I.; Crismari, D.V.; Balandin, A.A. Thermal Conductivity Inhibition in Phonon Engineered Core-Shell Cross-Section Modulated Si/Ge Nanowires. *Appl. Phys. Lett.* **2013**, *102*, 213109. [CrossRef]
30. Cocemasov, A.I.; Nika, D.L.; Fomin, V.M.; Grimm, D.; Schmidt, O.G. Phonon-Engineered Thermal Transport in Si Wires with Constant and Periodically Modulated Cross-Sections: A Crossover between Nano- and Microscale Regimes. *Appl. Phys. Lett.* **2015**, *107*, 011904. [CrossRef]
31. Melis, C.; Colombo, L. Lattice Thermal Conductivity of $Si_{1-x}Ge_x$ Nanocomposites. *Phys. Rev. Lett.* **2014**, *112*, 065901. [CrossRef]
32. Chen, J.; Zhang, G.; Li, B. Remarkable Reduction of Thermal Conductivity in Silicon Nanotubes. *Nano Lett.* **2010**, *10*, 3978–3983. [CrossRef]
33. Morata, A.; Pacios, M.; Gadea, G.; Flox, C.; Cadavid, D.; Cabot, A.; Tarancón, A. Large-Area and Adaptable Electrospun Silicon-Based Thermoelectric Nanomaterials with High Energy Conversion Efficiencies. *Nat. Commun.* **2018**, *9*, 1–8. [CrossRef] [PubMed]
34. Weng, W.; Yang, J.; Zhou, J.; Gu, D.; Xiao, W. Template-Free Electrochemical Formation of Silicon Nanotubes from Silica. *Adv. Sci.* **2020**, *7*, 2001492. [CrossRef]
35. Tseng, Y.M.; Gu, R.Y.; Cheng, S.L. Design and Fabrication of Vertically Aligned Single-Crystalline Si Nanotube Arrays and Their Enhanced Broadband Absorption Properties. *Appl. Surf. Sci.* **2020**, *508*, 145223. [CrossRef]
36. Sun, Y.-L.; Zheng, X.-D.; Jevasuwan, W.; Fukata, N. Silicon Nanotubes Fabricated by Wet Chemical Etching of ZnO/Si Core–Shell Nanowires. *Nanomaterials* **2020**, *10*, 2535. [CrossRef] [PubMed]
37. Liu, R.; Shen, C.; Dong, Y.; Qin, J.; Wang, Q.; Iocozzia, J.; Zhao, S.; Yuan, K.; Han, C.; Li, B. Sandwich-like CNTs/Si/C Nanotubes as High Performance Anode Materials for Lithium-Ion Batteries. *J. Mater. Chem. A* **2018**, *6*, 14797–14804. [CrossRef]
38. Jafari, M.A.; Kordbacheh, A.A.; Mahdian, S.; Ghasemi, N. Electronic and Transport Properties of (6, 2) Carbon and Silicon Nanotubes: A First-Principles Calculation. *Phys. E Low-Dimens. Syst. Nanostruct.* **2020**, *117*, 113855. [CrossRef]
39. Scarlet, S.P.; Vinodhkumar, N.; Srinivasan, R. Performance Enhancement of Junctionless Silicon Nanotube FETs Using Gate and Dielectric Engineering. *J. Comput. Electron.* **2021**, *20*, 209–217. [CrossRef]
40. Fomin, V.M. *Self-Rolled Micro-and Nanoarchitectures: Topological and Geometrical Effects*; Walter de Gruyter GmbH & Co KG: Berlin, Germany; Boston, MA, USA, 2021; ISBN 978-3-11-057557-6.
41. Grimm, D.; Wilson, R.B.; Teshome, B.; Gorantla, S.; Rümmeli, M.H.; Bublat, T.; Zallo, E.; Li, G.; Cahill, D.G.; Schmidt, O.G. Thermal Conductivity of Mechanically Joined Semiconducting/Metal Nanomembrane Superlattices. *Nano Lett.* **2014**, *14*, 2387–2393. [CrossRef]
42. Li, G.; Grimm, D.; Engemaier, V.; Lösch, S.; Manga, K.; Bandari, V.K.; Zhu, F.; Schmidt, O.G. Hybrid Semiconductor/Metal Nanomembrane Superlattices for Thermoelectric Application. *Phys. Status Solidi A* **2016**, *213*, 620–625. [CrossRef]
43. Li, G.; Yarali, M.; Cocemasov, A.; Baunack, S.; Nika, D.L.; Fomin, V.M.; Singh, S.; Gemming, T.; Zhu, F.; Mavrokefalos, A. In-Plane Thermal Conductivity of Radial and Planar Si/SiO_x Hybrid Nanomembrane Superlattices. *ACS Nano* **2017**, *11*, 8215–8222. [CrossRef]
44. Fomin, V.M.; Balandin, A.A. Phonon Spectrum Engineering in Rolled-up Micro-and Nano-Architectures. *Appl. Sci.* **2015**, *5*, 728–746. [CrossRef]
45. Dippong, T.; Cadar, O.; Levei, E.A.; Deac, I.G.; Goga, F.; Borodi, G.; Barbu-Tudoran, L. Influence of Polyol Structure and Molecular Weight on the Shape and Properties of $Ni_{0.5}Co_{0.5}Fe_2O_4$ Nanoparticles Obtained by Sol-Gel Synthesis. *Ceram. Int.* **2019**, *45*, 7458–7467. [CrossRef]
46. Dippong, T.; Cadar, O.; Levei, E.A.; Deac, I.G. Microstructure, Porosity and Magnetic Properties of $Zn_{0.5}Co_{0.5}Fe_2O_4/SiO_2$ Nanocomposites Prepared by Sol-Gel Method Using Different Polyols. *J. Magn. Magn. Mater.* **2020**, *498*, 166168. [CrossRef]
47. Agati, M.; Boninelli, S.; Castrucci, P.; Amiard, G.; Pandiyan, R.; Kolhatkar, G.; Dolbec, R.; Ruediger, A.; El Khakani, M.A. Formation of Silicon Nanocrystal Chains Induced via Rayleigh Instability in Ultrathin Si/SiO_2 Core/Shell Nanowires Synthesized by an Inductively Coupled Plasma Torch Process. *J. Phys. Mater.* **2018**, *2*, 15001. [CrossRef]
48. Zeng, L.; Liu, R.; Han, L.; Luo, F.; Chen, X.; Wang, J.; Qian, Q.; Chen, Q.; Wei, M. Preparation of a Si/SiO_2–Ordered-Mesoporous-Carbon Nanocomposite as an Anode for High-Performance Lithium-Ion and Sodium-Ion Batteries. *Chem. Eur. J.* **2018**, *24*, 4841–4848. [CrossRef] [PubMed]
49. Osminkina, L.A.; Žukovskaja, O.; Agafilushkina, S.N.; Kaniukov, E.; Stranik, O.; Gonchar, K.A.; Yakimchuk, D.; Bundyukova, V.; Chermoshentsev, D.A.; Dyakov, S.A. Gold Nanoflowers Grown in a Porous Si/SiO_2 Matrix: The Fabrication Process and Plasmonic Properties. *Appl. Surf. Sci.* **2020**, *507*, 144989. [CrossRef]
50. Du, M.; Bi, J.-Q.; Wang, W.-L.; Sun, X.-L.; Long, N.-N. Microstructure and Properties of SiO_2 Matrix Reinforced by BN Nanotubes and Nanoparticles. *J. Alloys Compd.* **2011**, *509*, 9996–10002. [CrossRef]
51. Anufriev, R.; Tachikawa, S.; Gluchko, S.; Nakayama, Y.; Kawamura, T.; Jalabert, L.; Nomura, M. Cross-Plane Thermal Conductivity in Amorphous Si/SiO_2 Superlattices. *Appl. Phys. Lett.* **2020**, *117*, 093103. [CrossRef]

52. Nika, D.L.; Zincenco, N.D.; Pokatilov, E.P. Lattice Thermal Conductivity of Ultra-Thin Freestanding Layers: Face-Centered Cubic Cell Model versus Continuum Approach. *J. Nanoelectron. Optoelectron.* **2009**, *4*, 170–173. [CrossRef]
53. Volz, S.G.; Chen, G. Molecular Dynamics Simulation of Thermal Conductivity of Silicon Nanowires. *Appl. Phys. Lett.* **1999**, *75*, 2056–2058. [CrossRef]
54. Glassbrenner, C.J.; Slack, G.A. Thermal Conductivity of Silicon and Germanium from 3K to the Melting Point. *Phys. Rev.* **1964**, *134*, A1058. [CrossRef]
55. Allen, P.B.; Feldman, J.L. Thermal Conductivity of Glasses: Theory and Application to Amorphous Si. *Phys. Rev. Lett.* **1989**, *62*, 645. [CrossRef] [PubMed]
56. Anderson, E.; Bai, Z.; Bischof, C.; Blackford, L.S.; Demmel, J.; Dongarra, J.; Du Croz, J.; Greenbaum, A.; Hammarling, S.; McKenney, A. *LAPACK Users' Guide*; SIAM: Philadelphia, PA, USA, 1999; ISBN 0-89871-447-8.
57. *GNU C Compiler*; Free Software Foundation: Boston, MA, USA, 2020.
58. Nishiguchi, N.; Ando, Y.; Wybourne, M.N. Acoustic Phonon Modes of Rectangular Quantum Wires. *J. Phys. Condens. Matter* **1997**, *9*, 5751. [CrossRef]
59. Zou, J.; Balandin, A. Phonon Heat Conduction in a Semiconductor Nanowire. *J. Appl. Phys.* **2001**, *89*, 2932–2938. [CrossRef]
60. Martin, P.; Aksamija, Z.; Pop, E.; Ravaioli, U. Impact of Phonon-Surface Roughness Scattering on Thermal Conductivity of Thin Si Nanowires. *Phys. Rev. Lett.* **2009**, *102*, 125503. [CrossRef]
61. Cocemasov, A.I.; Nika, D.L. Phonons and Phonon Thermal Conductivity in Silicon Nanolayers. *J. Nanoelectron. Optoelectron.* **2012**, *7*, 370–375. [CrossRef]
62. Fauziah, K.; Suzuki, Y.; Nogita, T.; Kamakura, Y.; Watanabe, T.; Salleh, F.; Ikeda, H. Effect of Phonon-Boundary Scattering on Phonon-Drag Factor in Seebeck Coefficient of Si Wire. *AIP Adv.* **2020**, *10*, 75015. [CrossRef]